Journal of Solid State Chemistry 184 (2011) 1499–1504

Contents lists available at ScienceDirect

Journal of Solid State Chemistry

journal homepage: www.elsevier.com/locate/jssc

The $La_{0.95}Ni_{0.6}Fe_{0.4}O_3$–$CeO_2$ system: Phase equilibria, crystal structure of components and transport properties

Elena Konysheva *, John T.S. Irvine

School of Chemistry, Purdie Building, University of St. Andrews, St. Andrews, Fife, KY16 9ST, UK

ARTICLE INFO

Article history:
Received 22 December 2010
Received in revised form
9 April 2011
Accepted 15 April 2011
Available online 22 April 2011

Keywords:
Perovskite
CeO_2
Phase equilibria
Conductivity

ABSTRACT

Phase equilibria, crystal structure, and transport properties in the $(100-x)$ $La_{0.95}Ni_{0.6}Fe_{0.4}O_3$–$xCeO_2$ (LNFCx) system (x=2–75 mol%) were studied in air. Evolution of phase compositions and crystal structure of components was observed. The LNFCx ($2 \le x \le 10$) are three-phase and comprise the perovskite phase with rhombohedral symmetry ($R\bar{3}c$), the modified ceria with fluorite structure ($Fm\bar{3}m$), and NiO as a secondary phase. These multiphase compositions exhibit metallic-like conductivity above 300 °C. Their conductivity gradually decreases from 395.6 to 260.6 S/cm, whereas the activation energy remains the same (E_a=0.04–0.05 eV), implying the decrease in the concentration of charge carriers. Phase compositions in the LNFCx ($25 \le x \le 75$) are more complicated. A change from semiconducting to metallic-like conductivity behavior was observed in LNFC25 at about 550 °C. The conductivity of LNFCx ($25 \le x \le 75$) could be explained in terms of a modified simple mixture model.
© 2011 Elsevier Inc. All rights reserved.

1. Introduction

Materials with perovskite and fluorite structures exhibit high electrical conductivity, good thermochemical stability under oxidizing atmosphere and have been considered for versatile technological applications (catalysts, membranes, electrodes, and electrolytes in power generating solid state devices) [1–4]. Good chemical compatibility of adjacent components (in particular in long term) is one of the challenges for the implementation of existing materials and the design of new ones. Different processes could occur at the interfaces between the adjacent components (interdiffusion of elements, preferable dissolution of certain element(s), evaporation or sorption of elements), and lead to a change in structural and transport properties of the adjacent components, thereby influencing the electrochemical performance of the whole system [5–10]. Therefore, it is necessary to know phase equilibria; structure of compounds formed and transport properties of multicomponent systems.

$LaNi_{1-y}Fe_yO_{3-\delta}$ perovskites are considered as promising materials for the application as an electrode and current collector in solid oxide fuel cells (SOFC) at intermediate temperatures due to their high metallic-like electrical conductivity [11]. The $LaNi_{0.6}Fe_{0.4}O_{3-\delta}$ perovskite has the highest electronic conductivity among $LaNi_{1-y}Fe_yO_3$ series. Besides, *A*-site deficient perovskites show a low capability of insulating phase formation at the interface with electrolytes, which could result in better long term electrochemical performance. Transport properties of CeO_2 based electrolytes have been actively explored to optimize their ionic conductivity [12–15]. $Ce_{1-x}Ln_xO_{2-\delta}$ (Ln=Gd, Sm, and $x \le 0.2$) compositions show the most promising transport properties [14]. Two-layered electrodes are generally used to enhance electrochemical performance of SOFC and minimize Cr-poisoning effect [16–18]. The outer layer of the two-layered electrodes is a perovskite phase, whereas the layer adjusted to the electrolyte is a mixture of the perovskite and electrolyte. This design would require good chemical stability at the phase interfaces in long term.

The simplified system $La_{0.95}Ni_{0.6}Fe_{0.4}O_3$–$CeO_2$ has been specially chosen in the present investigation to identify any interactions between major components (phase evolution and crystal structure of new phases) and study their electrical properties. The presence of a dopant in the $Ce_{1-x}Ln_xO_{2-\delta}$ electrolyte ($x \le 0.2$) may change the kinetics of phase evolution at the phase interfaces, but the La solubility in the fluorite structure of CeO_2 according to the literature [13,19] is much higher (up to 50 mol%) than the acceptor dopant concentration. This assumes that La redistribution between the main phases could occur and can be more accurately defined investigating the $La_{0.95}Ni_{0.6}Fe_{0.4}O_3$–$CeO_2$ system, although the absolute value of an additional La dissolution may alter depending on a dopant type and its concentration in cerium oxide.

2. Experimental

The initial perovskite $La_{0.95}Ni_{0.6}Fe_{0.4}O_3$ (LNF) was produced by combustion spray pyrolysis and supplied by PRAXAIR Inc., USA. CeO_2 delivered by ACROS ORGANICS (New Jersey, USA) was

* Corresponding author.
E-mail address: elena.konysheva@googlemail.com (E. Konysheva).

0022-4596/$ - see front matter © 2011 Elsevier Inc. All rights reserved.
doi:10.1016/j.jssc.2011.04.027

calcined at 1000 °C for 5 h to remove adsorbed water. The initial powders LNF and CeO_2 have comparable specific surface area: 6.00 and 2.34 m^2/g, respectively. Further, compositions in the following series $(100-x)$LNF · $xCeO_2$ (LNFC), where $x=2$, 5, 8, 10, 25, 50, and 75 mol%, were obtained by mechanical mixing of LNF and CeO_2 in mortar in relevant ratios, and followed by a calcination in air at 1350 °C for 5 h. The initial composition LNF was also calcined under the same conditions. The temperature of 1350 °C was specially chosen to enhance mobility of chemical elements and observe any changes in a phase composition and crystal structure within a shorter time scale. Although there is a general trend in the lowering of sintering temperature of ceramic units and operating temperature of solid oxide fuel cells, but this approach does not allow long term stability of multicomponent systems to be predicted.

X-ray powder diffraction (XRD) data were recorded in air at room temperature (RT) in transmission mode on a Stoe Stadi-P diffractometer with Cu$K\alpha$ radiation (Stoe & Cie GmbH, Germany) and for some nominal compositions in reflection mode on a Philips analytical X-ray PW1710 diffractometer with Cu$K\alpha$ radiation (Nederlandse Philips Bedrijven B.V., The Netherlands). The diffraction spectra for all samples were registered in the angular range of $15 \le 2\Theta \le 96$ with a step size of 0.1 and a recording time of 70 s for each step. Si powder (Alfa Aesar, Karlsruhe, Germany) was used as the external standard for the calibration of the diffractometer. The diffraction data were refined by the Rietveld method [20], using the Generalized Structure Analysis System (GSAS) program [21]. Electrical conductivity was measured on sintered pellets (rD~85% for LNFCx with $2 \le x \le 25$, 76% for LNFC50, and 73% for LNFC75) by the standard DC four terminal method between 50 and 900 °C in static air [22]. A current of 100 mA (Keithley model 220, USA) was applied in both directions and resistance was calculated as a gradient of potential *vs.* current. This was converted to conductivity using the geometrical factor of the sample.

3. Results and discussion

3.1. Phase equilibria and crystal structure at room temperature

According to neutron diffraction study [23], the *A*-site nominal composition $La_{0.95}Ni_{0.6}Fe_{0.4}O_{3-\delta}$ (LNF) comprises the cation stoichiometric phase $LaNi_{0.579}Fe_{0.421}O_3$ with rhombohedral structure (space group $R\bar{3}c$, no. 167) and 5.2 mol% NiO (space group $R\bar{3}m$, no. 166). The XRD analysis does not allow structural and quantitative characterization of NiO because only two very weak peaks could be observed in the XRD patterns recorded in the reflection mode. The peaks related to NiO phase are less discernible in the XRD patterns recorded in the transmission mode because of a high fluorescent background, Fig. 1a. CeO_2 has a fluorite-type structure (space group $Fm\bar{3}m$, no. 225) [24,25]. Very weak peak, which is close to the {1 1 1} cubic reflection of CeO_2, was observed in the XRD pattern of LNFC2, assuming a low solubility limit of CeO_2 in the perovskite structure. The LNFCx with 2 mol% $\le x \le$ 10 mol% are three phase: the perovskite phase with rhombohedral structure, the modified cerium oxide with fluorite

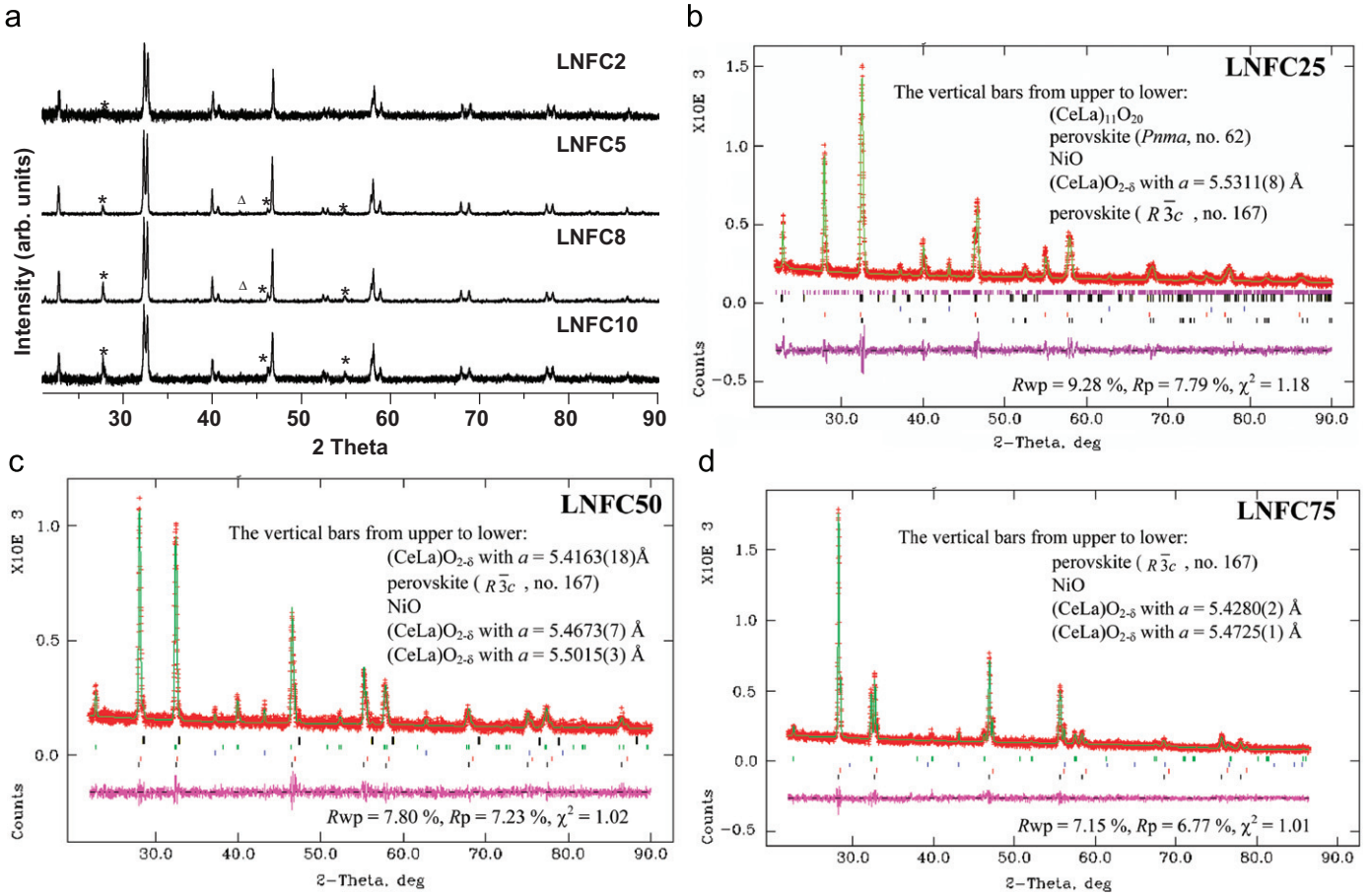

Fig. 1. Evolution of XRD patterns in the LNFC system at room temperature: (a) LNFC2, LNFC5; LNFC8, and LNFC10; the "∗" and "Δ" symbols indicate the peaks related to the modified ceria and NiO, respectively; (b) LNFC25; (c) LNFC50; and (d) LNFC75. Reliability factors are presented after the subtraction of the background. For (b)–(d): observed (cross symbols), calculated (continuous line), and difference profiles (bottom line). Vertical bars show calculated reflections for different phases. XRD patterns were recorded in the transmission mode.

structure (space group $Fm\bar{3}m$, no. 225) and NiO, Fig. 1a. The lattice parameters and unit cell volume of the perovskite phase are nearly constant within this concentration range, Fig. 2a and c. Intensity of diffraction peaks related to the modified cerium oxide increases gradually, Fig. 1a. The lattice parameter of the modified cerium oxide varies between 5.5300(10) and 5.5371(4) Å (Fig. 2b), which is much higher than for undoped CeO_2 and formally corresponds to the dissolution of ~37–38 mol% La in the fluorite structure [13,19]. A preferable dissolution of La cations with a larger ionic radius ($r^{VIII}_{La^{3+}} = 1.18$ Å and $r^{VIII}_{Ce^{4+}} = 0.80$ Å) [26] in the fluorite structure seems to occur. A formation of any ternary compounds was not observed in the La_2O_3–NiO and La_2O_3–CeO_2–NiO systems fabricated at 1200 °C [27,28], but the formation of a solid solution $Ce_{0.9}Ni_{0.1}O_2$ (fabricated through a soft-chemistry route and finally calcinated at 1500 °C) was suggested [29]. Our compositions were fabricated at 1350 °C, thereby implying that a small fraction of Ni cations may dissolve in the fluorite lattice. The intensity of peaks related to NiO in the LNFC*x* (2 mol% ≤ *x* ≤ 10 mol%) is very small to characterize this phase.

The phase compositions in LNFC25, LNFC50, and LNFC75 are more complicated. According to the refinement at least five phases present in LNFC25, Fig. 1b. Beside a perovskite phase with rhombohedral structure ($R\bar{3}c$, no. 167) and NiO, the presence of a perovskite phase with orthorhombic structure (*Pnma*, no. 62: $a=5.493(3)$ Å, $b=7.840(6)$ Å, $c=5.515(4)$ Å, and $V=237.49(8)$ Å) was observed. The reliability factors and χ^2 are better if the *B*-sites in the perovskite phase with rhombohedral structure are occupied by Ni cations, whereas the *B*-sites in the perovskite phase with orthorhombic structure are occupied by Fe cations, which correlates with the data reported in the literature [30,31]: the end members of the $LaNiO_3$–$LaFeO_3$ system exhibit rhombohedral and orthorhombic symmetries, respectively. The change in symmetry from rhombohedral to orthorhombic in the $LaNi_{1-x}Fe_xO_3$ series occurs when $x > 0.5$ [32]. The lattice parameter of the modified cerium oxide ($Fm\bar{3}m$) in LNFC25 equals to 5.5311(8) Å, which corresponds formally to the La dissolution (up to 35 mol%) in the fluorite structure [13,19]. The relative intensity of the two peaks related to NiO becomes slightly stronger, Fig. 1b, which may imply a partial decomposition of the perovskite phase or dissolution of NiO from the perovskite structure. A phase $(CeLa)_{11}O_{20}$ with triclinic structure ($P-1$, no. 2: $a=6.7813(8)$ Å, $b=10.2608(10)$ Å, $c=6.7781(8)$ Å, $\alpha=89.671(9)^\circ$, $\beta=99.62(1)^\circ$, $\lambda=96.129(8)^\circ$, and $V=462.31(6)$ Å^3) was also revealed. Oxygen deficiency in cerium oxides could be stabilized by dissolution of cations with lower oxidation states. The presence of Ce_6O_{11} and $(CeLaSrCo)_{11}O_{20}$ phases was revealed, respectively, in $La_{0.6}Ce_{0.4}CoO_3$ by XRD [33] and in 57 mol% $La_{0.6}Sr_{0.4}CoO_3$–43 mol% CeO_2 composition by high-resolution transmission electron microscopy [7]. La replacing Ce gives oxygen deficiency without need for reduction. Due to dissolution of La cations with a larger ionic radius the unit cell volume of $(CeLa)_{11}O_{20}$ is higher compared to $Ce_{11}O_{20}$ with $V=457.10(38)$ Å [34]. The accuracy of the refinement for LNFC25 was better with $(CeLa)_{11}O_{20}$ ($R_{wp}=9.28\%$, $R_p=7.79\%$, and $\chi^2=1.18$) compared to that without $(CeLa)_{11}O_{20}$ ($R_{wp}=13.27\%$, $R_p=10.29\%$, and $\chi^2=1.55$). In the case of LNFC50, phases $(CeLa)O_{2-\delta}$ with the fluorite structure (space group $Fm\bar{3}m$, no. 225) with $a=5.5015(3)$ Å (the major fraction, formally corresponds to the dissolution of ~30 mol% La), $a=5.4673(7)$ Å (formally corresponds to the dissolution of ~15 mol% La), and $a=5.4163(18)$ Å (minor fraction, the lattice parameter is very close to that for pure CeO_2) coexists beside NiO and the perovskites phase with rhombohedral structure, Fig. 1c and Supporting information. An existence of $(CeLa)O_{2-\delta}$ phases with different lattice parameters could be as a result of an inhomogeneous distribution of La cations. On the other hand, the formation of $FeCe_2O_4$ and $CeFeO_3$ compounds with Ce^{3+} and Fe^{2+} was reported in the literature [35,36], which may indicate a possibility of Fe cation dissolution in cerium oxide. Therefore, one cannot exclude that at a higher temperature (1350 °C), some fractions of Fe cations and Ni cations (individually or simultaneously) dissolve in the fluorite structure, thereby stabilizing certain compositions. The dissolution of Fe cations in the fluorite structure could inhibit the formation of the perovskite phase with orthorhombic symmetry. The phases formed seem to be highly disordered because the noticeable improvement in the reliability factors and χ^2 were achieved when anisotropic displacement parameters were introduced in the refinement. In addition, we considered the phase models including the perovskite phase with orthorhombic symmetry (*Pnma*) or $(CeLa)_{11}O_{20}$, but the accuracy of the refinements did not become better. The four phases were revealed in LNFC75: highly disordered $(CeLa)O_{2-\delta}$ phases with the fluorite structure ($Fm\bar{3}m$) with $a=5.4725(1)$ Å (the main fraction) and $a=5.4280(2)$ Å; the perovskite phase with rhombohedral structure ($R\bar{3}c$) and NiO.

The lattice parameters of the perovskite phase with rhombohedral structure ($R\bar{3}c$) in LNFC10, LNFC25, LNFC50, and LNFC75 change gradually: the *a* lattice parameter increases whereas the β angle decreases, Fig. 2a. The unit cell volume of the perovskite phase with rhombohedral structure ($R\bar{3}c$) increases gradually (Fig. 2c) that could be caused by the combination of several

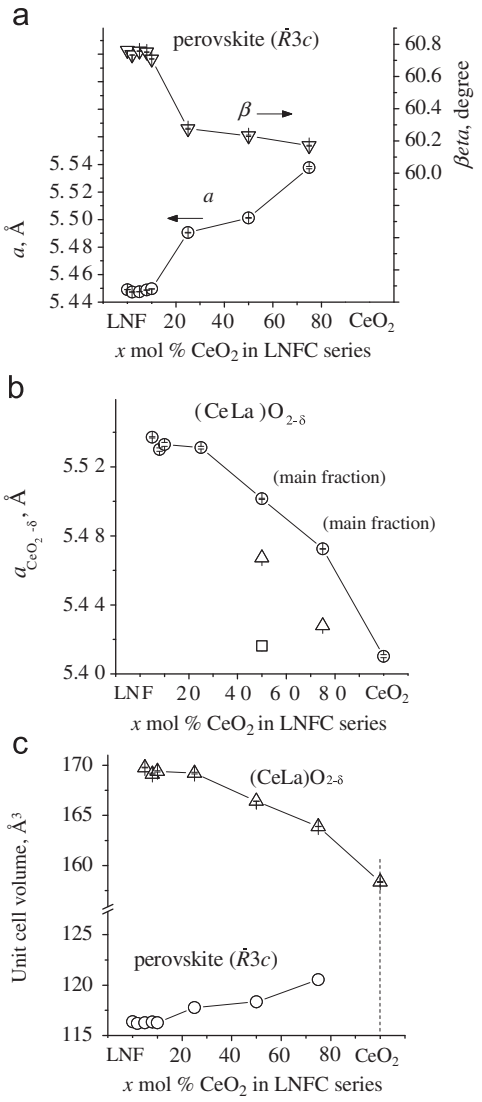

Fig. 2. Evolution of the structural parameters of the dominant phases in the LNFC series at room temperature: (a) the lattice parameters of the perovskite phase with rhombohedral structure ($R\bar{3}c$); (b) the lattice parameter of the modified ceria with fluorite structure ($Fm\bar{3}m$); and (c) their unit cell volumes. Error bars are within the symbols. The lattice parameters of LNF are presented from Ref. [23].

factors: (i) a certain increase in Fe occupancy on the *B*-site, (ii) increase in a fraction of Ni^{2+} cations on the *B*-site (Ni^{2+} has a larger ionic radius compared to Ni^{3+} [26] and the perovskite lattice can support some fraction of Ni^{2+} cations on the *B*-sites [23]), and (iii) a change in oxygen stoichiometry of the perovskite phase and in the tilting angle. The *a* lattice parameter and unit cell volume of the main fraction of the modified cerium oxide $(CeLa)O_{2-\delta}$ decrease in a non-linear way (Fig. 2b), implying more complex dissolution behavior. This result is not surprising for ternary or more complex system. Only in the case of a mixture of two simple oxides/phases, structural parameters expect to be constant, and this does not necessary hold where three or more phases are involved. The less the fraction of the perovskite phase in the LNFC compositions, the less the fraction of La cations would be available for the dissolution. At the same time, a fraction of CeO_2 increases. Therefore, the fraction of La cations available for the dissolution in the unit cell volume of cerium oxide will decrease, resulting in the decrease in the lattice parameter.

Fig. 3 illustrates the evolution of O–O distances in the LNFC system for the perovskite phase with rhombohedral structure ($R\bar{3}c$) and for the main fraction of the $(CeLa)O_{2-\delta}$ with fluorite structure ($Fm\bar{3}m$) obtained from the refinement of the XRD patterns recorded in the transmission mode. For LNFC25 and LNFC50, the differences between O–O distances in the modified cerium oxide and one set of O–O distances in the perovskite phase

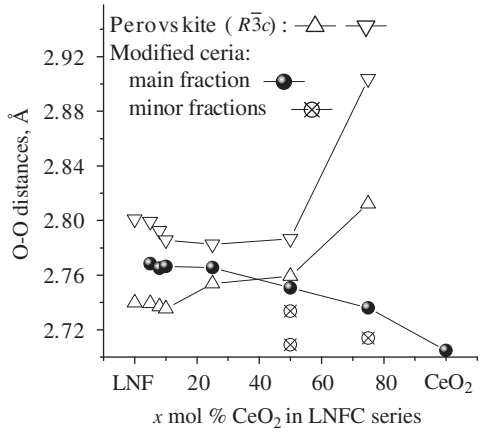

Fig. 3. Evolution of O–O distances in the LNFC system at room temperature for the perovskite phase with rhombohedral structure ($R\bar{3}c$) and for a series of $(CeLa)O_{2-\delta}$ solid solutions with cubic structure ($Fm\bar{3}m$). Error bars are within the symbols.

($R\bar{3}c$) amount to 0.0113 and 0.0092 Å, respectively, thereby implying the possibility of an interfacial interaction between these phases through the oxygen sublattice. Similar structural behavior was also observed in the $La_{0.6}Sr_{0.4}CoO_3$–CeO_2 composite system [7]. The adjusting of the oxygen sublattices related to different structure seems to be caused by the dissolution of La and Sr (only for $La_{0.6}Sr_{0.4}CoO_3$–CeO_2 system) from the perovskite phase into the fluorite structure. In contrast, this effect was not revealed in the $La_{0.8}Sr_{0.2}MnO_3$–CeO_2 system [37]. The dissolution of La and Sr from $La_{0.8}Sr_{0.2}MnO_3$ into the fluorite structure of CeO_2 was negligible.

3.2. Conductivity in air

The electrical conductivity in the LNFC system ($a_{(O_2)} = 0.21$) is shown in Fig. 4a as a function of the reciprocal temperature. The conductivity of all compositions investigated is reversible on the heating/cooling cycle. A change from semiconducting to metallic-like conductivity behavior was observed for $LaNi_{0.6}Fe_{0.4}O_3$ (LNF) above 300 °C [11,21]. The nominal compositions LNFC*x* (2 mol% ≤ $x \leq 10$ mol%) that have the same lattice parameters show metallic-like conductivity behavior above 300–350 °C similar to LNF (Supporting information). A change from semiconducting to metallic-like conductivity behavior was observed for LNFC25 around 550 °C. The lattice parameters of the perovskite phase with rhombohedral symmetry in LNFC25 increase, which could be caused by both Ni exsolution from the perovskite lattice and increase in the fraction of Ni^{2+} cations on the *B* site, and result in complex conductivity behavior with the temperature variation. Metallic-like conductivity was observed in the substituted $LaNiO_3$ if the Ni occupancy on the B sublattice is higher than 50 mol% ($LaFe_{1-x}Ni_xO_3$ [11], $La_{0.9}Sr_{0.1}Ga_{1-x}Ni_xO_3$ [38], and $La_{0.935}Sr_{0.02}Ni_{0.54}Fe_{0.36}Mn_{0.1}O_3$ [39]). The change from the small polaron hopping mechanism to the small polaron band mechanism could occur with the rising temperature in the materials with high Ni occupancy (50–60 mol%) [40]. The continuousness of the 3*d* Ni-3*d* Ni band, in this case, would be very sensitive to the Ni–Ni bond length, fraction of Ni^{2+} cations, and the number of Ni neighbors. LNF reduced under argon at 800 °C, which contains higher fraction of Ni^{2+} cations on the *B*-sites [23], shows metallic-like behavior only above 700 °C [41]. LNFC50 and LNFC75 compositions have a lower fraction of the perovskite phase and exhibit a semiconducting behavior in the whole temperature range investigated.

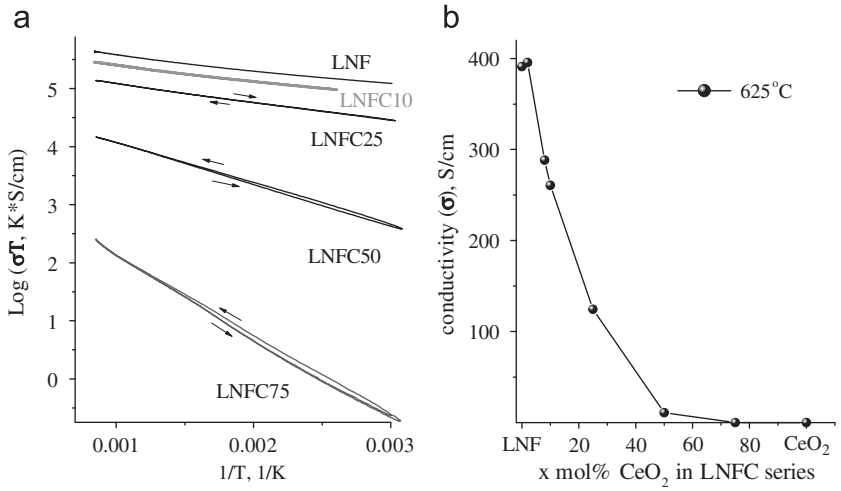

Fig. 4. Conductivity of compositions in the LNFC series, $a_{(O_2)} = 0.21$: (a) temperature dependence of conductivity, the heating/cooling rate is 3 °C/min; and (b) compositional dependence of conductivity at 625 °C.

Table 1
Apparent activation energy (for regions with semiconducting type of conductivity).

Composition	E_a (eV)
LNF	0.04 ± 0.001 (50–300 °C)
LNFC2	0.05 ± 0.001 (50–300 °C)
LNFC08	0.04 ± 0.001 (50–300 °C)
LNFC10	0.05 ± 0.001 (50–350 °C)
LNFC25	0.07 ± 0.003 (50–550 °C)
LNFC50	0.15 ± 0.01 (50–900 °C)
LNFC75	0.28 ± 0.01 (50–900 °C)

The electrical conductivity of LNFC compositions as a function of CeO_2 content has the same trend in the temperature range of 50–900 °C, Fig. 4b. Data for the bulk conductivity of CeO_2 were taken from Ref. [42]. The electrical conductivity of LNF and LNFC2 is comparable and it decreases gradually with further rise in CeO_2 concentration up to 10 mol%: 395.6 S/cm (LNFC2), 288.2 S/cm (LNFC8), and 260.6 S/cm (LNFC10) at 625 °C. The dominate perovskite phase with rhombohedral structure in the LNFC*x* ($2\ \text{mol\%} \le x \le 10\ \text{mol\%}$) has the same lattice parameters, implying that the presence of secondary phase(s) could affect the electronic conductivity of these compositions. The presence of NiO as a secondary phase in a small concentration (5 mol% or less) could give little dilution effect [43]. In contrast to LNF, cerium oxide is a fast ionic conductor with oxygen vacancies and electrons as the main charge carriers [44,45]. Decrease in the conductivity observed for LNFC8 and LNFC10 is stronger than it would be expected from the dilution effect. Similar values of the apparent activation energy (E_a), Table 1, were revealed for these compositions, which could imply the decrease in the concentration of charge carrying holes. The recombination of electrons from the modified cerium oxide and holes from the perovskite phase could occur at phase interfaces, leading to the depletion of charge carriers and suppressing the electronic conductivity. This could occur independently of whether charge transfer pathways cross phase interfaces or not [7].

In spite of the complex phase composition, LNFC25 exhibits a relatively high value of the electronic conductivity (124.5 S/cm at 625 °C) with a low value of the activation energy, Table 1. For comparison, the electronic conductivity of $La_{0.8}Sr_{0.2}MnO_3$ and $La_{0.65}Sr_{0.3}MnO_3$ at 800 °C varies within 80–100 S/cm with $E_a = 0.11$ eV ($La_{0.8}Sr_{0.2}MnO_3$) [37,46]. These compounds possess the highest electronic conductivity among manganites with a different level of Sr doping and *A*-site deficiency [46,47]; and they are being actively tested as the cathode materials in solid oxide fuel cells [4,48,49]. The conductivity of LNFC50 and LNFC75 decreases further: 10.9 and 0.1 S/cm at 625 °C, respectively. The apparent activation energy increases gradually from 0.07 eV (LNFC25) to 0.28 eV for LNFC75. The latest value is comparable with $E_a = 0.22$ eV reported for the electronic hopping transport in the polycrystalline $CeO_{2-\delta}$ (assuming a low level of δ and small polaron mechanism) [50]. However, the conductivity of LNFC75 at 625 °C is higher by about three orders of magnitude than for undoped CeO_2 and lower by about three orders of magnitude than for LNF. Probably the conductivity of the LNFC*x* ($25\ \text{mol\%} \le x \le 75\ \text{mol\%}$) could be explained in terms of a simple mixture model and not a percolation model considering in addition (i) evolution of phase composition in the LNFC series, (ii) the expansion of the perovskite phase with rhombohedral structure accompanied by the increase in the polaron hopping distances, and (iii) concentration and type of the main charge carriers in the modified cerium oxide, which relates directly to the recombination of charge carriers at phase interfaces.

4. Conclusions

Diverse phase compositions and evolution of the crystal structure of components were observed in the $(100-x)$ $La_{0.95}Ni_{0.6}Fe_{0.4}O_3$–$xCeO_2$ (LNFC) system fabricated under oxidizing atmosphere. Previous investigation showed that A-site deficient nominal composition $La_{0.95}Ni_{0.6}Fe_{0.4}O_3$ can be represented as a mixture of the cation stoichiometric perovskite phase and NiO as a secondary phase. The solubility limit of cerium oxide (cubic symmetry, $Fm\bar{3}m$) in the perovskite structure is less than 2 mol%, and the LNFC*x* ($2\ \text{mol\%} \le x \le 10\ \text{mol\%}$) are three phase, consisting of the perovskite phase, the modified cerium oxide and NiO. The modification of the CeO_2 occurs mainly due to the dissolution of La from the perovskite phase. The electrical conductivity of these compositions is high enough for their application as cathode materials in the solid oxide fuel cell systems at intermediate temperatures. In spite of the complex phase composition and evolution of the lattice parameters of the dominate perovskite phase with rhombohedral structure, LNFC25 exhibits slightly higher electrical conductivity and a lower value of the activation energy compared to those for the traditionally used Mn containing perovskites. The formal comparison of the lattice parameter of the modified ceria (major fraction) in LNFC*x* ($2 \le x \le 50$) with the literature data known for the $Ce_{1-x}La_xO_{2-\delta}$ could assume that ~30–38 mol% La dissolves in the fluorite structure, which exceeds the dopant concentration in the $Ce_{1-x}Ln_xO_{2-\delta}$ electrolyte and may suggest the La cations redistribution at the phase interfaces during long term operation.

Acknowledgments

The authors gratefully acknowledge EPSRC for financial support.

Appendix A. Supplementary material

Supplementary data associated with this article can be found in the online version at doi:10.1016/j.jssc.2011.04.027.

References

[1] A. Trovarelli, Catal. Rev. Sci. Eng. 38 (1996) 439–520.
[2] E.A. Lombardo, M.A. Ulla, Res. Chem. Intermed. 24 (1998) 581–592.
[3] J.A. Kilner, Faraday Discuss. 134 (2007) 9–15.
[4] N.Q. Minh, J. Am. Ceram. Soc. 76 (1993) 563–588.
[5] H. Schmalzried, Chemical Kinetics of Solids, VCH, Weinheim, Germany, 1995, p. 422.
[6] J.R. Tolchard, T. Grande, Solid State Ionics 178 (2007) 593–599.
[7] E. Konysheva, R. Blackley, J.T.S. Irvine, Chem. Mater. 22 (2010) 4700–4711.
[8] E. Konysheva, U. Seeling, A. Besmehn, L. Singheiser, K. Hilpert, J. Mater. Sci. 42 (2007) 5778–5784.
[9] S.P. Jiang, Solid State Ionics 146 (2002) 1–22.
[10] E. Konysheva, H. Penkalla, E. Wessel, J. Mertens, U. Seeling, L. Singheiser, K. Hilpert, J. Electrochem. Soc. 153 (2006) A765–A773.
[11] R. Chiba, F. Yoshimura, Y. Sakurai, Solid State Ionics 124 (1999) 281–288.
[12] D.L. Maricle, T.E. Swarr, S. Karavolis, Solid State Ionics 52 (1992) 173–182.
[13] H. Yamamura, E. Katoh, M. Ichikawa, K. Kakinuma, T. Mori, H. Haneda, Electrochemistry 68 (2000) 455–459.
[14] M. Mogensen, N.M. Sammes, G.A. Tompsett, Solid State Ionics 129 (2000) 63–94.
[15] W. Preis, J. Waldhäusl, A. Egger, W. Sitte, E. De Carvalho, J.T.S. Irvine, ECS Trans. 25 (2) (2009) 1635–1642.
[16] M. Juhl, S. Primdahl, C. Manon, M. Mogensen, J. Power Sources 61 (1996) 173–181.
[17] E. Konysheva, J. Mertens, H. Penkalla, L. Singheiser, K. Hilpert, J. Electrochem. Soc. 154 (2007) B1252–B1264.
[18] R. Chiba, H. Orui, T. Komatsu, Y. Tabata, K. Nozawa, M. Arakawa, K. Sato, H. Arai, J. Electrochem. Soc. 155 (2008) B575–B580.
[19] B.C. Morris, W.R. Flavell, W.C. Mackrodt, M.A. Morris, J. Mater. Chem. 3 (1993) 1007–1013.
[20] H.M. Rietveld, Acta Crystallogr. 22 (1967) 151–152.

[21] A.C. Larson, R.B. von Dreele, GSAS—Generalized Structure Analysis System; Los Alamos National Laboratory Report LAUR-86-748, Los Alamos National Laboratory, Los Alamos, NM, 1994.
[22] E. Konysheva, J.T.S. Irvine, J. Mater. Chem. 18 (2008) 5147–5154.
[23] E. Konysheva, E. Suard, J.T.S. Irvine, Chem. Mater. 21 (2009) 5307–5318.
[24] JCPDS, International Centre for Diffraction Data, file No. 34-0394.
[25] M. Yashima, S. Kobayashi, T. Yasui, Solid State Ionics 177 (2006) 211–215.
[26] R.D. Shannon, C.T. Rewitt, Acta Cryst. B 25 (1969) 925–946.
[27] M. Hrovat, J. Holc, S. Bernik, D. Makovec, Mater. Res. Bull. 33 (1998) 1175–1183.
[28] M. Hrovat, J. Holc, Z. Samardzija, S. Bernik, J. Mater. Sci. Lett. 19 (2000) 233–235.
[29] B.G. Pound, Solid State Ionics 52 (1992) 183–188.
[30] J.A.M. Van Roosmalen, E.H.P. Cordfunke, J. Solid State Chem. 93 (1991) 212–219.
[31] S. Geller, E.A. Wood, Acta Crystallogr. 9 (1956) 563–568.
[32] H. Falcon, A.E. Goeta, G. Punte, R.E. Carbonio, J. Solid State Chem. 133 (1997) 379–385.
[33] Y. Wen, C. Zhang, H. He, Y. Yu, Y. Teraoka, Catal. Today 126 (2007) 400–405.
[34] Inorganic crystal structures database, file ICSD-88758, 〈http://cds.dl.ac.uk/icsd/index.php〉 (last access—June 2010).
[35] B.F. Belov, A.V. Goroh, V.P. Demchuk, N.A. Dorschenko, Z.A. Somojlenko, Inorg. Mater. 19 (1983) 231–234.
[36] M. Robbins, G.K. Wertheim, A. Menth, R.C. Sherwood, J. Phys. Chem. Solids 30 (1969) 1823–1825.
[37] E. Konysheva, J.T.S. Irvine, A. Besmehn, Solid State Ionics 180 (2009) 778–783.
[38] N.J. Long, F. Lecarpentier, H.L. Tuller, Electroceramics 3 (1999) 399–407.
[39] E. Konysheva, J.T.S. Irvine, A. Besmehn, Solid State Ionics 179 (2008) 1432–1435.
[40] E. Konysheva, J.T.S. Irvine, Chem. Mater. 23 (2011) 1841–1850.
[41] E. Konysheva, J.T.S. Irvine, J. Power Sources 193 (2009) 175–179.
[42] E. Konysheva, J.T.S. Irvine, Solid State Ionics 184 (2011) 27–30.
[43] J. Knudsen, P.B. Friehling, N. Bonanos, Solid State Ionics 176 (2005) 1563–1569.
[44] P. Kofstad, Nonstoichiometry, Diffusion and Electrical Conductivity in Binary Metal Oxides, John Wiley & Sons Inc., New York, 1972, p. 276.
[45] H.L. Tuller, A.S. Nowick, J. Electrochem. Soc. 126 (1979) 209–217.
[46] H. Ullmann, N. Trofimenko, F. Tietz, D. Stover, A. Ahmad-Khanlou, Solid State Ionics 138 (2000) 79–90.
[47] J.H. Kuo, H.U. Anderson, D.M. Sparlin, J. Solid State Chem. 87 (1990) 55–63.
[48] J. Fleig, Annu. Rev. Mater. Res. 33 (2003) 361–382.
[49] E. Konysheva, J. Laatsch, E. Wessel, F. Tietz, N. Christiansen, L. Singheiser, K. Hilpert, Solid State Ionics 177 (2006) 923–930.
[50] R.N. Blumenthal, R.L. Hofmaier, J. Electrochem. Soc. 121 (1974) 126–131.